Journal of Magnetic Resonance **151,** 298–313 (2001)
doi:10.1006/jmre.2001.2382, available online at http://www.idealibrary.com on IDEAL®

Dynamics of Spin $I = 3/2$ under Spin-Locking Conditions in an Ordered Environment

J. R. C. van der Maarel,* W. Jesse,* I. Hancu,† and D. E. Woessner‡

*Soft Condensed Matter Group, Leiden Institute of Chemistry, Leiden University, P.O. Box 9502, 2300 RA Leiden, The Netherlands; †Department of Physics, University of Pittsburgh, Pittsburgh, Pennsylvania 15213; and ‡Department of Radiology, Rogers Magnetic Resonance Center, The University of Texas Southwestern Medical Center at Dallas, Dallas, Texas 75235-9085

Received December 26, 2000; revised April 25, 2001

We have derived approximate analytic solutions to the master equation describing the evolution of the spin $I = 3/2$ density operator in the presence of a radio-frequency (RF) field and both static and fluctuating quadrupolar interactions. Spectra resulting from Fourier transformation of the evolutions of the on-resonance spin-locked magnetization into the various coherences display two satellite pairs and, in some cases, a central line. The central line is generally trimodal, consisting of a narrow component related to a slowly relaxing mode and two broad components pertaining to two faster relaxing modes. The rates of the fast modes are sensitive to slow molecular motion. Neither the amplitude nor the width of the narrow component is affected by the magnitude of the static coupling, whereas the corresponding features of the broad components depend in a rather complicated manner on the spin-lock field strength and static quadrupolar interaction. Under certain experimental conditions, the dependencies of the amplitudes on the dynamics are seen to vanish and the relaxation rates reduce to relatively simple expressions. One of the promising emerging features is the fact that the evolutions into the selectively detected quadrupolar spin polarization order and the rank-two double-quantum coherence do not exhibit a slowly relaxing mode and are particularly sensitive to slow molecular motion. Furthermore, these coherences can only be excited in the presence of a static coupling and this makes it possible to discern nuclei in anisotropic from those in isotropic environment. The feasibility of the spin-lock pulse sequences with limited RF power and a nonvanishing average electric field gradient has been demonstrated through experiments on sodium in a dense lyotropic DNA liquid crystal.

Key Words: **nuclear magnetic relaxation; quadrupolar nuclei; spin-locking; multiple-quantum spectroscopy; sodium imaging, DNA, lyotropic liquid crystal.**

INTRODUCTION

Quadrupolar spin probes are becoming increasingly important in a wide range of applications from the investigation of soft condensed matter such as (bio)polymers in the liquid state (*1–4*), through biological fluids (*5*), to the diagnosis of pathology in humans *via* MRI (*6*). Another application is the study of surface properties of porous materials with xenon-131 (*7*). Among those probes, the naturally occurring spin quantum number 3/2 nuclei ^{7}Li, ^{23}Na, ^{39}K, ^{87}Rb, ^{35}Cl, ^{81}Br, and ^{131}Xe constitute an important class, for which the spin dynamics can be solved in closed analytical form (*8–10*). The magnetic relaxation of these nuclei provides a mechanism to extract information about molecular motions (*11*). Longitudinal relaxation gives information about relatively fast motions, whereas slow dynamics is probed more efficiently by applying a lock through an on-resonance radio frequency (RF) field. In previous works, one of us has analyzed the relaxation of a system of spin $I = 3/2$ under (pulsed) spin locking, which allows to sample the spectral density of the fluctuating quadrupolar interactions at a frequency of the order of the RF field strength (*12–14*). The formerly derived formalism is strictly valid however for nuclei in an isotropic environment, where the nuclei experience a zero average electric field gradient. In many important systems, including biological tissue and lyotropic liquid crystals, the quadrupolar interaction is not completely averaged by molecular motion in times less than the inverse Larmor frequency and the NMR spectra display a residual, possibly hidden, quadrupolar splitting. Accordingly, to extend the range of applications to this important class of materials, it is necessary to include the static quadrupolar Hamiltonian in the calculation of the destiny of the density operator in the presence of a RF field.

A second motivation to consider the effects of relaxation during RF excitation originates from the increasing importance of sodium MRI in whole body scanners (*15*). In particular, the use of triple-quantum filtered images over a relatively large field of view (>15 cm) requires rather long ($\pi/2$) RF pulses on the order of 0.5 ms. In previous work, the unwanted signal loss during such long RF pulses was predicted with a model for the dynamics of spin $I = 3/2$ in biological media (*16*). Following the formalism for spin $I = 1$ nuclei (*17*), we have derived the differential equations describing the evolution of the spin $I = 3/2$ density operator in the presence of a RF field and both static and fluctuating quadrupolar interactions. These equations were subsequently numerically integrated to successfully predict the experimental 15% signal loss in the triple-quantum filtered spectra of a piece of bovine nasal cartilage when the ($\pi/2$) RF pulse

1090-7807/01 $35.00

width was increased from 0.1 to 0.5 ms (the flip-angle was kept constant with a concurrent decrease in RF power). Although the differential equations are readily amenable by numeric methods, approximate analytic solutions under certain simplifying assumptions might be convenient for a general understanding of the spin dynamics. Apart from their relevance in the context of extracting the spectral densities of the fluctuating quadrupolar interaction, these approximate solutions might also facilitate the optimization of the MR imaging techniques to selectively detect ions involved in slow motion and/or in anisotropic environment.

A third possible use of applying a RF field during more extended time-intervals comes from the need to discern different pools (e.g., intra- versus extra-cellular) of ions in biological systems. For instance, it has been suggested that certain pathologic conditions (such as cartilage degenerative diseases) correlate well to changes in the spectra of sodium ions involved in slow motion (*18*). Several methods have been proposed to detect sodium ions in an anisotropic environment. Among those, the most common methods are the double-quantum magic angle (DQ-MA) filter and the Jeener–Broekaert sequence (*5, 19, 20*). We will show here that quadrupolar spin polarization order, as well as rank-two double-quantum coherences are excited in the presence of a RF field, provided the amplitude of the spin lock field is on the same order of magnitude as the residual quadrupolar coupling. Accordingly, the selective detection of the quadrupolar polarization or the rank-two double-quantum coherence after applying a RF lock is proposed to be an alternative MRI filtering technique for monitoring ordered ions in, e.g., human skeletal muscle or brain *in vivo* (*21*).

The outline of this paper is as follows. First, we will reiterate the necessary differential equations describing the time-evolution of the density operator. These equations are subsequently solved without relaxation effects to provide for a reference in the perturbation analysis of the lineshapes. After a discussion of the fast relaxing modes, which are most sensitive to slow molecular motion, we will present some practical considerations how to selectively detect the various coherences. Finally, the feasibility of the various pulse sequences is demonstrated with some experiments on sodium in a dense lyotropic DNA liquid crystal.

DIFFERENTIAL EQUATIONS

The differential equations describing the dynamics of the spin $I = 3/2$ density operator in the simultaneous presence of a static quadrupolar coupling and a RF field have been derived and reported in previous work (*16*). For ease of reference, we sketch the derivation and reiterate the pertinent equations necessary for an analysis of the spin-lock experiment. All calculations are done in the Larmor frequency-rotating frame, indicated by an asterisk. The time-evolution of the density operator under a static Hamiltonian H_S^* and a fluctuating quadrupolar interaction Hamiltonian $H_{QF}^*(t)$ is given by the master equation (*22*)

$$\frac{d\sigma^*}{dt} = -i[H_S^*, \sigma^*] + f(\sigma^*) \qquad [1]$$

with the Redfield relaxation superoperator

$$f(\sigma^*) = -\int_0^\infty \langle [H_{QF}^*(t), [e^{-iH_S^*\tau} H_{QF}^*(t-\tau) e^{iH_S^*\tau}, \sigma^*(t)]] \rangle \, d\tau. \qquad [2]$$

Note the presence of the static Hamiltonian H_S^* in the relaxation contribution, which cannot be neglected if H_S^* does not commute with $H_{QF}^*(t)$.

We express the density operator and the Hamiltonians in terms of irreducible tensor operators (*23*). Symmetric and antisymmetric combinations are defined as

$$\begin{aligned} T_{lm}(s) &= 1/\sqrt{2}(T_{l-m} + T_{lm}) \\ T_{lm}(a) &= 1/\sqrt{2}(T_{l-m} - T_{lm}). \end{aligned} \qquad [3]$$

Orthonormal tensor operators $\hat{T}_{lm}$ are also introduced, which fulfill the orthogonality relationship $Tr\{\hat{T}_{lm}\hat{T}^\dagger_{l'm'}\} = \delta_{ll'}\delta_{mm'}$ with $\hat{T}^\dagger_{lm} = (-1)^m \hat{T}_{l-m}$. The unit tensors are related to their T_{lm} counterparts according to $\hat{T}_{lm} = a_l T_{lm}$. For spin $I = 3/2$, the coefficients a_l have the values $a_0 = 1/2$, $a_1 = 1/\sqrt{5}$, $a_2 = 1/2\sqrt{2/3}$, and $a_3 = 1/3\sqrt{2}$. Symmetric and anti-symmetric combinations of the unit tensors are defined analogously to Eq. [3]. The density operator is expanded in 16 basis operators: $\hat{T}_{00}$ (the identity), $\hat{T}_{10}$ (longitudinal magnetization), $\hat{T}_{11}(a)$ and $\hat{T}_{11}(s)$ (proportional to the x- and y-magnetization, respectively), $\hat{T}_{20}$ (quadrupolar spin polarization), $\hat{T}_{21}(s)$ and $\hat{T}_{21}(a)$ (rank-two single-quantum coherences), $\hat{T}_{22}(s)$ and $\hat{T}_{22}(a)$ (rank-two double-quantum coherences), $\hat{T}_{30}$ (octopolar spin polarization), $\hat{T}_{31}(s)$ and $\hat{T}_{31}(a)$ (rank-three single-quantum coherences), $\hat{T}_{32}(s)$ and $\hat{T}_{32}(a)$ (rank-three double-quantum coherences) and $\hat{T}_{33}(s)$ and $\hat{T}_{33}(a)$ (rank-three triple-quantum coherences).

With respect to the Larmor frequency-rotating frame, the Zeeman Hamiltonian ($H_z = \omega_0 I_z = \omega_0 T_{10}$) vanishes. The time-independent Hamiltonian is then given by the sum of the static quadrupolar and RF contributions:

$$H_S^* = H_{QS}^* + H_1^*. \qquad [4]$$

The static quadrupolar Hamiltonian commutes with the Zeeman Hamiltonian and takes the form

$$H_{QS}^* = \frac{1}{6}\omega_Q [3I_z^2 - I(I+1)] = \omega_Q \hat{T}_{20}, \qquad [5]$$

where ω_Q denotes the residual quadrupolar interaction parameter. The latter coupling parameter represents the part of the quadrupolar interaction that persists after motional averaging and is not to be confused with the root mean-square-average of the fluctuating part. With the RF field applied exactly on resonance along the x axis with field strength $\omega_1 = -\gamma B_1$, the corresponding Hamiltonian reads

$$H_1^* = \omega_1 I_x = \sqrt{5}\omega_1 \hat{T}_{11}(a). \quad [6]$$

The zero-average fluctuating quadrupolar interaction can be expressed as

$$H_{QF}^*(t) = C_Q \sum_{m=-2}^{2} (-1)^m T_{2m} e^{im\omega_0 t}[F_{2-m}(t) - \langle F_{2-m}\rangle]. \quad [7]$$

Here, $C_Q = \sqrt{6}\,eQ/(2I(2I-1)\hbar) = eQ/(\hbar\sqrt{6})$ (Q is the quadrupolar moment of the nucleus, the other symbols have their usual meaning), the electric field gradient tensor components, F_{2m}, are defined elsewhere (*24*), and $\langle F_{2m}\rangle$ represents their average value.

With the commutation relations (*23*) and neglecting relaxation, Eq. [1] reduces to two sets of coupled differential equations. The first is

The matrices in Eqs. [8] and [9] can be diagonalized and the differential equations can subsequently be integrated in analytical form. The resulting time-dependencies of the basis operators have been set out by Campolieti *et al.* (*25*). The matrix in Eq. [8] has a three-dimensional null space spanned by three eigenvectors with eigenvalues being equal to zero. Furthermore, the remaining eigenvalues

$$\begin{aligned} \pm i\lambda_1 &= \pm i\sqrt{\omega_Q^2 + 2\omega_1\omega_Q + 4\omega_1^2} \\ \pm i\lambda_2 &= \pm i\sqrt{\omega_Q^2 - 2\omega_1\omega_Q + 4\omega_1^2} \end{aligned} \quad [10]$$

are imaginary and correspond to two sets of resonance frequencies, each set with equal magnitude but opposite signs. Accordingly, spectra resulting from Fourier transformation of the time dependencies of the operators in Eq. [8] display a central resonance and two satellite pairs related to the zero and imaginary eigenvalues, respectively (as will be shown below, the spectra pertaining to the $\hat{T}_{21}(s)$ and $\hat{T}_{32}(a)$ coherences show two satellite pairs only and no central line). The matrix in Eq. [9] has eight imaginary eigenvalues

$$\begin{aligned} \pm i\lambda_3 &= \pm i\left(\omega_1 + 1/\sqrt{2}\sqrt{\omega_Q^2 + 4\omega_1^2 + \lambda_1\lambda_2}\right) \\ \pm i\lambda_4 &= \pm i\left(\omega_1 + 1/\sqrt{2}\sqrt{\omega_Q^2 + 4\omega_1^2 - \lambda_1\lambda_2}\right) \end{aligned}$$

$$\frac{d}{dt}\begin{pmatrix} \hat{T}_{11}(a) \\ \hat{T}_{20} \\ \hat{T}_{21}(s) \\ \hat{T}_{22}(s) \\ \hat{T}_{31}(a) \\ \hat{T}_{32}(a) \\ \hat{T}_{33}(a) \end{pmatrix} = \begin{pmatrix} 0 & 0 & i\sqrt{3/5}\omega_Q & 0 & 0 & 0 & 0 \\ 0 & 0 & -i\sqrt{3}\omega_1 & 0 & 0 & 0 & 0 \\ i\sqrt{3/5}\omega_Q & -i\sqrt{3}\omega_1 & 0 & -i\omega_1 & i\sqrt{2/5}\omega_Q & 0 & 0 \\ 0 & 0 & -i\omega_1 & 0 & 0 & i\omega_Q & 0 \\ 0 & 0 & i\sqrt{2/5}\omega_Q & 0 & 0 & -i\sqrt{5/2}\omega_1 & 0 \\ 0 & 0 & 0 & i\omega_Q & -i\sqrt{5/2}\omega_1 & 0 & -i\sqrt{3/2}\omega_1 \\ 0 & 0 & 0 & 0 & 0 & -i\sqrt{3/2}\omega_1 & 0 \end{pmatrix} \begin{pmatrix} \hat{T}_{11}(a) \\ \hat{T}_{20} \\ \hat{T}_{21}(s) \\ \hat{T}_{22}(s) \\ \hat{T}_{31}(a) \\ \hat{T}_{32}(a) \\ \hat{T}_{33}(a) \end{pmatrix} \quad [8]$$

and for the second set one has

$$\frac{d}{dt}\begin{pmatrix} \hat{T}_{10} \\ \hat{T}_{11}(s) \\ \hat{T}_{21}(a) \\ \hat{T}_{22}(a) \\ \hat{T}_{30} \\ \hat{T}_{31}(s) \\ \hat{T}_{32}(s) \\ \hat{T}_{33}(s) \end{pmatrix} = \begin{pmatrix} 0 & -i\omega_1 & 0 & 0 & 0 & 0 & 0 & 0 \\ -i\omega_1 & 0 & i\sqrt{3/5}\omega_Q & 0 & 0 & 0 & 0 & 0 \\ 0 & i\sqrt{3/5}\omega_Q & 0 & -i\omega_1 & 0 & i\sqrt{2/5}\omega_Q & 0 & 0 \\ 0 & 0 & -i\omega_1 & 0 & 0 & 0 & i\omega_Q & 0 \\ 0 & 0 & 0 & 0 & 0 & -i\sqrt{6}\omega_1 & 0 & 0 \\ 0 & 0 & i\sqrt{2/5}\omega_Q & 0 & -i\sqrt{6}\omega_1 & 0 & -i\sqrt{5/2}\omega_1 & 0 \\ 0 & 0 & 0 & i\omega_Q & 0 & -i\sqrt{5/2}\omega_1 & 0 & -i\sqrt{3/2}\omega_1 \\ 0 & 0 & 0 & 0 & 0 & 0 & -i\sqrt{3/2}\omega_1 & 0 \end{pmatrix} \begin{pmatrix} \hat{T}_{10} \\ \hat{T}_{11}(s) \\ \hat{T}_{21}(a) \\ \hat{T}_{22}(a) \\ \hat{T}_{30} \\ \hat{T}_{31}(s) \\ \hat{T}_{32}(s) \\ \hat{T}_{33}(s) \end{pmatrix}. \quad [9]$$

$$\pm i\lambda_5 = \pm i\left(\omega_1 - 1/\sqrt{2}\sqrt{\omega_Q^2 + 4\omega_1^2 + \lambda_1\lambda_2}\right)$$
$$\pm i\lambda_6 = \pm i\left(\omega_1 - 1/\sqrt{2}\sqrt{\omega_Q^2 + 4\omega_1^2 - \lambda_1\lambda_2}\right) \qquad [11]$$

and the corresponding spectra show 4 satellite pairs and no central resonance.

The time-independent Hamiltonian H_s^* can however be neglected in the relaxation terms proportional to the spectral densities at approximately one and two times the Larmor frequency. This is because ω_0 is generally much larger than any of the frequencies λ_i and, hence, $J_m(m\omega_0 \pm \lambda_i) \approx J_m(m\omega_0) = J_m$ for $m = \pm 1$ and ± 2. The $m = 0$ term in the relaxation contribution is sensetive to slowly fluctuating electric field gradients, and H_S^* has now explicitly to be taken into acount. The resulting time-evolution of the density matrix under relaxation takes on the form (*16*)

$$\frac{d}{dt}\begin{pmatrix} \hat{T}_{11}(a) \\ \hat{T}_{20} \\ \hat{T}_{21}(s) \\ \hat{T}_{22}(s) \\ \hat{T}_{31}(a) \\ \hat{T}_{32}(a) \\ \hat{T}_{33}(a) \end{pmatrix} = -\begin{pmatrix} 3/10D + J_1 + 2/5J_2 & 0 & 0 & -\sqrt{15}/10E & \sqrt{6}/10D - \sqrt{6}/5J_2 & 0 & 0 \\ 3\sqrt{5}/10A & 2J_1 + 2J_2 & 0 & \sqrt{3}/2B & \sqrt{30}/10A & 0 & 0 \\ 0 & 0 & 3/2G + J_1 + 2J_2 & 0 & 0 & 3/2F & 0 \\ 3\sqrt{15}/10F & 0 & 0 & 3/2G + 2J_1 + J_2 & 3\sqrt{10}/10F & 0 & 0 \\ 3\sqrt{6}/20I - \sqrt{6}/5J_2 & 0 & 0 & 3\sqrt{10}/20J & 3/10I + J_1 + 3/5J_2 & 0 & 0 \\ 0 & 0 & 3/2F & 0 & 0 & 3/2G + J_2 & 0 \\ 3\sqrt{10}/20B & 0 & 0 & \sqrt{6}/4A & \sqrt{15}/10B & 0 & J_1 + J_2 \end{pmatrix}\begin{pmatrix} \hat{T}_{11}(a) \\ \hat{T}_{20} \\ \hat{T}_{21}(s) \\ \hat{T}_{22}(s) \\ \hat{T}_{31}(a) \\ \hat{T}_{32}(a) \\ \hat{T}_{33}(a) \end{pmatrix} \qquad [13]$$

and

$$\frac{d}{dt}\begin{pmatrix} \hat{T}_{10} \\ \hat{T}_{11}(s) \\ \hat{T}_{21}(a) \\ \hat{T}_{22}(a) \\ \hat{T}_{30} \\ \hat{T}_{31}(s) \\ \hat{T}_{32}(s) \\ \hat{T}_{33}(s) \end{pmatrix} = -\begin{pmatrix} 2/5J_1 + 8/5J_2 & 0 & \sqrt{15}/10A & 0 & 4/5J_1 - 4/5J_2 & 0 & \sqrt{15}/5B & 0 \\ 0 & 3/10C + J_1 + 2/5J_2 & 0 & -\sqrt{15}/10A & 0 & \sqrt{6}/10C - \sqrt{6}/5J_2 & 0 & 0 \\ 0 & 0 & 3/2G + J_1 + 2J_2 & 0 & 0 & 0 & 0 & 0 \\ 0 & 0 & 0 & 3/2\,G + 2J_1 + J_2 & 0 & 0 & 0 & 0 \\ 4/5J_1 - 4/5J_2 & 0 & \sqrt{15}/5A & 0 & 8/5J_1 + 2/5J_2 & 0 & -\sqrt{15}/10B & 0 \\ 0 & 3\sqrt{6}/20H - \sqrt{6}/5J_2 & 0 & 3\sqrt{10}/20A & 0 & 3/10H + J_1 + 3/5J_2 & 0 & 0 \\ 0 & 0 & 0 & 0 & 0 & 0 & 3/2G + J_2 & 0 \\ 0 & 3\sqrt{10}/20B & 0 & \sqrt{6}/4A & 0 & \sqrt{15}/10B & 0 & J_1 + J_2 \end{pmatrix}\begin{pmatrix} \hat{T}_{10} \\ \hat{T}_{11}(s) \\ \hat{T}_{21}(a) \\ \hat{T}_{22}(a) \\ \hat{T}_{30} \\ \hat{T}_{31}(s) \\ \hat{T}_{32}(s) \\ \hat{T}_{33}(s) \end{pmatrix}. \qquad [14]$$

Relaxation effects can be incorporated into the differential equations through the addition of the relaxation contribution to the master equation. This contribution has been derived in previous work, including the effect of the static Hamiltonian in the relaxation superoperator (*16*). The relaxation contribution reduces to a combination of the spectral densities $J_m(m\omega_0 \pm \lambda_i)$ at a number of frequencies $m\omega_0 \pm \lambda_i$ with $m = 0, \pm 1, \pm 2$ and λ_i given by Eqs. [10] and [11]. The imaginary part of the spectral density function results in very small, second-order, frequency shifts and in a weak coupling of the two sets of differential equations. These dynamic frequency shifts are commonly ignored. The real part of the spectral density is defined as the (cosine) Fourier transform of the electric field gradient correlation function.

$$J_m(\omega) = \left(\frac{eQ}{\hbar}\right)^2 \frac{1}{2}\int_{-\infty}^{\infty} \langle [F_{2m}^*(t) - \langle F_{2m}^*\rangle] \times [F_{2m}(t-\tau) - \langle F_{2m}\rangle]\rangle \exp(i\omega\tau)\, d\tau. \qquad [12]$$

The coefficients A through J are linear combinations of the spectral densities at frequencies λ_1, λ_2, and zero: $J_0(\lambda_1) = J_{\lambda 1}$, $J_0(\lambda_2) = J_{\lambda 2}$, and $J_0(0) = J_0$, respectively. The coefficients of these combinations are collected in Table 1. The frequencies λ_1 and λ_2 are related to both the residual quadrupolar coupling and the (tunable) RF field strength according to Eq. [10]. Due to the presence of the RF field, the invariance of the spin system under a rotation about the z axis is lifted. This results in a different relaxation behavior of the symmetric and anti-symmetric tensor combinations. In the absence of a low frequency dispersion, i.e., when $J_0(0) \approx J_0(\lambda_1) \approx J_0(\lambda_2) = J_0$, the ω_Q and ω_1 dependencies in the rates Eqs. [13] and [14] vanish and the matrices reduce to the much simpler forms in terms of J_0, J_1, and J_2 only and are listed in Ref. (*16*). Without RF, the ω_Q dependence in the rates vanishes, because the static quadrupolar Hamiltonian Eq. [5] commutes with the $m = 0$ term in the fluctuating quadrupolar Hamiltonian Eq. [7].

The total time-dependence of the basis operators is given by the sums of Eqs. [8] and [13], and Eqs. [9] and [14]. These two sets of equations evolve independently, but they are coupled at

TABLE 1
Coefficients in Eqs. [13] and [14] in Terms of the Spectral Densities $J_0(\lambda_1)$, $J_0(\lambda_2)$, and $J_0(0)$

	$J_0(\lambda_1)$	$J_0(\lambda_2)$	$J_0(0)$
A	$\frac{\omega_1(\omega_Q+\omega_1)}{\lambda_1^2}$	$\frac{\omega_1(\omega_Q-\omega_1)}{\lambda_2^2}$	$-\frac{2\omega_1\omega_Q\left(\omega_Q^2+2\omega_1^2\right)}{\lambda_1^2\lambda_2^2}$
B	$-\frac{\omega_1(\omega_Q+\omega_1)}{\lambda_1^2}$	$\frac{\omega_1(\omega_Q-\omega_1)}{\lambda_2^2}$	$-\frac{2\omega_1^2\left(\omega_Q^2-4\omega_1^2\right)}{\lambda_1^2\lambda_2^2}$
C	$-\frac{\omega_1(\omega_Q-2\omega_1)}{\lambda_1^2}$	$\frac{\omega_1(\omega_Q+2\omega_1)}{\lambda_2^2}$	$\frac{2\left(\omega_Q^4+8\omega_1^4\right)}{\lambda_1^2\lambda_2^2}$
D	$\frac{\omega_1(\omega_Q+4\omega_1)}{\lambda_1^2}$	$-\frac{\omega_1(\omega_Q-4\omega_1)}{\lambda_2^2}$	$\frac{2\omega_Q^2\left(\omega_Q^2+2\omega_1^2\right)}{\lambda_1^2\lambda_2^2}$
E	$\frac{\omega_1(\omega_Q+4\omega_1)}{\lambda_1^2}$	$\frac{\omega_1(\omega_Q-4\omega_1)}{\lambda_2^2}$	$-\frac{2\omega_1\omega_Q\left(\omega_Q^2-4\omega_1^2\right)}{\lambda_1^2\lambda_2^2}$
F	$-\frac{\omega_1^2}{\lambda_1^2}$	$\frac{\omega_1^2}{\lambda_2^2}$	$-\frac{4\omega_1^3\omega_Q}{\lambda_1^2\lambda_2^2}$
G	$\frac{\omega_1^2}{\lambda_1^2}$	$\frac{\omega_1^2}{\lambda_2^2}$	$\frac{2}{3}\left[\frac{\omega_Q^4+\omega_Q^2\omega_1^2+4\omega_1^4}{\lambda_1^2\lambda_2^2}\right]$
H	$\frac{\omega_1(\omega_Q+3\omega_1)}{\lambda_1^2}$	$-\frac{\omega_1(\omega_Q-3\omega_1)}{\lambda_2^2}$	$\frac{2}{3}\left[\frac{2\omega_Q^4+5\omega_Q^2\omega_1^2-4\omega_1^4}{\lambda_1^2\lambda_2^2}\right]$
I	$-\frac{\omega_1(\omega_Q-\omega_1)}{\lambda_1^2}$	$\frac{\omega_1(\omega_Q+\omega_1)}{\lambda_2^2}$	$\frac{2}{3}\left[\frac{2\omega_Q^4-\omega_Q^2\omega_1^2+20\omega_1^4}{\lambda_1^2\lambda_2^2}\right]$
J	$\frac{\omega_1(\omega_Q-\omega_1)}{\lambda_1^2}$	$\frac{\omega_1(\omega_Q+\omega_1)}{\lambda_2^2}$	$-\frac{2\omega_1\omega_Q\left(\omega_Q^2+6\omega_1^2\right)}{\lambda_1^2\lambda_2^2}$

a change of RF phase. Once the eigenvalues and eigenoperators are known, the time-dependence of each of the basis operators can be determined. The time-evolution can be solved in analytical form in two limiting situations. In the absence of a RF field, the results are given by, among others, Dinesen and Sanctuary (*26*) and one of the present authors (*24*). Without quadrupolar splitting ($\omega_Q = 0$), the relaxation under (pulsed) spin-locking in the doubly rotating (toggling) tilted frame has been analyzed in previous work (*12–14*). In the simultaneous presence of RF and a static quadrupolar coupling, the master equation cannot be solved in analytical form. Although the eigensystems are readily amenable by numeric methods, approximate analytic solutions under certain simplifying assumptions might be convenient for an understanding of the spin dynamics. For this purpose, we will first analyze the time-dependence of the density operator without relaxation effects in the context of the spin-lock experiment. The effects of relaxation will subsequently be treated as a first order, time-independent, perturbation to the static Hamiltonian H_S^* (*27*).

UNPERTURBED TIME-DEPENDENCE UNDER THE STATIC HAMILTONIAN

In a $T_{1\rho}$ experiment, the density operator is initially prepared in a $\hat{T}_{11}(a)$ state (proportional to x-magnetization) by a hard $(\pi/2)_y$ pulse followed by a spin-lock pulse with field strength B_1 along the x axis (some experimental considerations are given below). The first set of coupled differential equations (i.e., the sum of Eqs. [8] and [13]) contains $\hat{T}_{11}(a)$ and is hence relevant for a description of the spin-lock experiment. We will now analyze the corresponding eigensystem and the resulting time-evolution of $\hat{T}_{11}(a)$ under the static Hamiltonian H_S^* only.

Without relaxation, the time-evolution of the relevant subset of the density operator is given by Eq. [8]. The seven eigenvalues and eigenoperators of the matrix are, respectively (*16*),

$$
\begin{aligned}
0 \quad & A_1 = \sqrt{\frac{5}{2}}\frac{\omega_1^2}{\omega_Q^2}\hat{T}_{11}(a) + \sqrt{\frac{3}{2}}\frac{\omega_1}{\omega_Q}\hat{T}_{22}(s) + \hat{T}_{33}(a) \\
0 \quad & A_2 = \left(\frac{5\omega_1^2}{\sqrt{6}\omega_Q^2} - \sqrt{\frac{2}{3}}\right)\hat{T}_{11}(a) + \sqrt{\frac{5}{2}}\frac{\omega_1}{\omega_Q}\hat{T}_{22}(s) + \hat{T}_{31}(a) \\
0 \quad & A_3 = \sqrt{5}\frac{\omega_1}{\omega_Q}\hat{T}_{11}(a) + \hat{T}_{20} \qquad [15]
\end{aligned}
$$

$$
\begin{aligned}
\mp i\lambda_1 \quad A_{\mp 4} = {} & \sqrt{\frac{2}{5}}\frac{\omega_Q}{\omega_1}\hat{T}_{11}(a) - \sqrt{2}\hat{T}_{20} \mp \sqrt{\frac{2}{3}}\frac{\lambda_1}{\omega_1}\hat{T}_{21}(s) \\
& - \sqrt{\frac{2}{3}}\left(1 + \frac{\omega_Q}{\omega_1}\right)\hat{T}_{22}(s) + \frac{1}{\sqrt{15}}\left(5 + \frac{2\omega_Q}{\omega_1}\right) \\
& \times \hat{T}_{31}(a) \pm \sqrt{\frac{2}{3}}\frac{\lambda_1}{\omega_1}\hat{T}_{32}(a) + \hat{T}_{33}(a)
\end{aligned}
$$

$$
\begin{aligned}
\mp i\lambda_2 \quad A_{\mp 5} = {} & -\sqrt{\frac{2}{5}}\frac{\omega_Q}{\omega_1}\hat{T}_{11}(a) + \sqrt{2}\hat{T}_{20} \pm \sqrt{\frac{2}{3}}\frac{\lambda_2}{\omega_1}\hat{T}_{21}(s) \\
& + \sqrt{\frac{2}{3}}\left(1 - \frac{\omega_Q}{\omega_1}\right)\hat{T}_{22}(s) + \frac{1}{\sqrt{15}}\left(5 - \frac{2\omega_Q}{\omega_1}\right) \\
& \times \hat{T}_{31}(a) \pm \sqrt{\frac{2}{3}}\frac{\lambda_2}{\omega_1}\hat{T}_{32}(a) + \hat{T}_{33}(a)
\end{aligned}
$$

with λ_1 and λ_2 given in Eq. [10]. With eigensystem Eq. [15], the unperturbed time-evolution of $\hat{T}_{11}(a)$ takes on the form

$$
\begin{aligned}
& e^{iH_S^*t}\hat{T}_{11}(a)e^{-iH_S^*t} \\
& \quad = a_{11}(t)\hat{T}_{11}(a) + a_{20}(t)\hat{T}_{20} + a_{21}(t)\hat{T}_{21}(s) + a_{22}(t)\hat{T}_{22}(s) \\
& \qquad + a_{31}(t)\hat{T}_{31}(a) + a_{32}(t)\hat{T}_{32}(a) + a_{33}(t)\hat{T}_{33}(a) \qquad [16]
\end{aligned}
$$

and the coefficients $a_{ij}(t)$ are set out in Table 2. Spectra resulting from the Fourier transform of the time-evolutions into the various (indicated) coherences are displayed in Fig. 1. These spectra were calculated by numerically solving Eqs. [8] and [13] with the density operator in the initial $\hat{T}_{11}(a)$ state and including relaxation effects as detailed below. The resonance positions and integrated intensities are given by the coefficients $a_{ij}(t)$ in Table 2. In particular, the spectra

TABLE 2
Coefficients Giving the Time-Dependence of $\hat{T}_{11}(a)$ under H_S^*

$a_{11}(t)$	$\frac{1}{10}\left[\frac{4\left(\omega_Q^4+4\omega_Q^2\omega_1^2+40\omega_1^4\right)}{\lambda_1^2\lambda_2^2}+3\omega_Q^2\left(\frac{\cos\lambda_1 t}{\lambda_1^2}+\frac{\cos\lambda_2 t}{\lambda_2^2}\right)\right]$
$a_{20}(t)$	$\frac{3\omega_Q\omega_1}{2\sqrt{5}}\left(\frac{2\left(\omega_Q^2+4\omega_1^2\right)}{\lambda_1^2\lambda_2^2}-\frac{\cos\lambda_1 t}{\lambda_1^2}-\frac{\cos\lambda_2 t}{\lambda_2^2}\right)$
$a_{21}(t)$	$\frac{i\sqrt{3}\omega_Q}{2\sqrt{5}}\left(\frac{\sin\lambda_1 t}{\lambda_1}+\frac{\sin\lambda_2 t}{\lambda_2}\right)$
$a_{22}(t)$	$-\frac{\sqrt{3}\omega_Q}{2\sqrt{5}}\left[\frac{2\omega_1\left(\omega_Q^2-4\omega_1^2\right)}{\lambda_1^2\lambda_2^2}+\frac{(\omega_Q+\omega_1)\cos\lambda_1 t}{\lambda_1^2}-\frac{(\omega_Q-\omega_1)\cos\lambda_2 t}{\lambda_2^2}\right]$
$a_{31}(t)$	$-\frac{\sqrt{3}\omega_Q}{10\sqrt{2}}\left[\frac{4\omega_Q\left(\omega_Q^2-\omega_1^2\right)}{\lambda_1^2\lambda_2^2}-\frac{(2\omega_Q+5\omega_1)\cos\lambda_1 t}{\lambda_1^2}-\frac{(2\omega_Q-5\omega_1)\cos\lambda_2 t}{\lambda_2^2}\right]$
$a_{32}(t)$	$-\frac{i\sqrt{3}\omega_Q}{\sqrt{5}}\left(\frac{\sin\lambda_1 t}{\lambda_1}-\frac{\sin\lambda_2 t}{\lambda_2}\right)$
$a_{33}(t)$	$\frac{3\omega_Q\omega_1}{2\sqrt{10}}\left(\frac{4\omega_Q\omega_1}{\lambda_1^2\lambda_2^2}+\frac{\cos\lambda_1 t}{\lambda_1^2}-\frac{\cos\lambda_2 t}{\lambda_2^2}\right)$

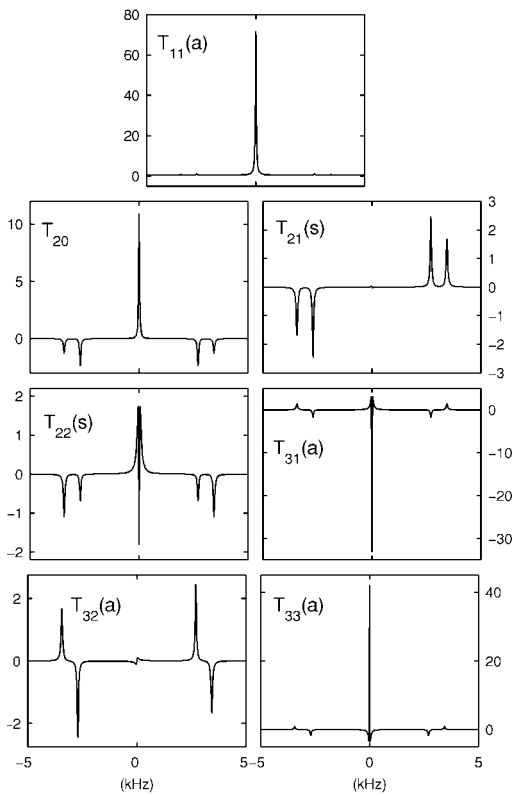

FIG. 1. Simulated spectra resulting from the Fourier transform of the numerically solved time-evolution Eqs. [8] and [13]. The density operator is prepared in a $\hat{T}_{11}(a)$ state (proportional to x-magnetization) by an initial hard $(\pi/2)_y$ pulse followed by a 90° phase shift. The detected coherences are indicated. The spectral densities are calculated with a slow mode correlation time $\omega_Q\tau_S = 0.1$ and root-mean-square coupling constant $\chi_S = 2.5$ kHz, together with a high frequency contribution $\alpha = (x_F^2\tau_F)/(x_S^2\tau_S) = 0.1$. The other parameters are $\omega_Q/2\pi = 0.75$ kHz and $\omega_1/2\pi = 1.5$ kHz $(\omega_1/\omega_Q = 2)$.

corresponding to the $\hat{T}_{11}(a)$, $\hat{T}_{20}$, $\hat{T}_{22}(s)$, $\hat{T}_{31}(a)$, and $\hat{T}_{33}(a)$ coherences show a prominent central resonance and two satellite pairs at frequencies λ_1 and λ_2, respectively (for $\hat{T}_{11}(a)$ the intensities of the satellites are negligibly small with the present parameters). A central resonance is absent in the signals pertaining to $\hat{T}_{21}(s)$ and $\hat{T}_{32}(a)$, which display two satellite pairs in anti-phase only. The remaining coherences [i.e., $\hat{T}_{10}$, $\hat{T}_{11}(s)$, $\hat{T}_{21}(a)$, $\hat{T}_{22}(a)$, $\hat{T}_{30}$, $\hat{T}_{31}(s)$, $\hat{T}_{32}(s)$, and $\hat{T}_{33}(s)$] belong to the other subset (with a time-evolution determined by Eqs. [9] and [14]) and are irrelevant in the context of the spin-lock experiment. Furthermore, the Fourier transforms of the conversions into the latter coherences display four satellite pairs only (at frequencies given by Eq. [11]) and no central line (spectra not shown).

Satellites are liable to line-broadening effects related to inhomogeneity in B_1 field strength and/or a distribution in static quadrupolar coupling across the sample. Accordingly, the central lines in the spectra pertaining to the $\hat{T}_{11}(a)$, $\hat{T}_{20}$, $\hat{T}_{22}(s)$, $\hat{T}_{31}(a)$, and $\hat{T}_{33}(a)$ coherences are designated for relaxation studies. The shapes of these central lines are determined by the perturbation of the nullspace of the matrix in Eq. [8]. The nullspace is spanned by the three eigenoperators A_1, A_2, and A_3 with zero eigenvalue (the nullity is 3). As a result of the perturbation by the relaxation terms, the originally degenerate eigenvalues cease to be degenerate and the singularity is removed. The central resonance becomes hence multimodal; i.e., it consists of a sum of Lorentzians with different widths and amplitudes. The maximum number of modes equals the nullity 3. The widths and amplitudes follow from the numeric integration of the sum of Eqs. [8] and [13], but in the next section we will derive solutions under the condition that the linewidths are much smaller than any of the frequencies λ_1 and λ_2. This

condition can always be arranged with a sufficiently intense RF field strength. We will analyze the relaxation behavior with time-independent first-order perturbation theory for a system where the unperturbed operator has a discrete spectrum of degenerate and nondegenerate eigenvalues (*27*).

PERTURBATION ANALYSIS OF THE LINE-SHAPES

Under the condition that the linewidths are much smaller than the frequencies λ_1 and λ_2, the operators corresponding with the nonsingular eigenvalues in Eq. [15] are to a very good approximation still eigenoperators if the relaxation contribution Eq. [13] is included. The operators $A_{\pm 4}$ and $A_{\pm 5}$ oscillate with frequencies $\pm\lambda_1$ and $\pm\lambda_2$, respectively, and are decoupled and relax independently from any other eigenoperator. For these decoupled operators, the relaxation rates are given by the real part of the diagonal elements of the master equation in the (approximate) eigenoperator representation Eq. [15] (the imaginary part gives the frequencies). These real parts of the diagonal elements read

$$A_{\pm 4}: \frac{(\omega_Q+\omega_1)^2}{\lambda_1^2} J_0 + \frac{3\omega_1^2}{2\lambda_1^2} J_{\lambda_1} + J_1 + \frac{2\omega_Q^2+4\omega_Q\omega_1+11\omega_1^2}{2\lambda_1^2} J_2$$

$$A_{\pm 5}: \frac{(\omega_Q-\omega_1)^2}{\lambda_2^2} J_0 + \frac{3\omega_1^2}{2\lambda_2^2} J_{\lambda_2} + J_1 + \frac{2\omega_Q^2-4\omega_Q\omega_1+11\omega_1^2}{2\lambda_2^2} J_2. \quad [17]$$

The rates of the satellite pairs at frequencies $\pm\lambda_1$ and $\pm\lambda_2$ are readily identified with the rates of the operators $A_{\pm 4}$ and $A_{\pm 5}$, respectively. The relative intensities are given by the results in Table 2. However, signals originating from the satellites have little practical value due to the additional line-broadening effects given by B_1 field inhomogeneity and/or distribution in static quadrupolar coupling.

The operators A_1, A_2, and A_3 are coupled and their degeneracy is removed by the relaxation contribution. They are however decoupled from $A_{\pm 4}$ and $A_{\pm 5}$, if the central resonance does not overlap with the satellites. The corresponding subset of the master equation in the operator representation Eq. [15] (the secular terms) can be diagonalized and subsequently integrated in analytical form. For this purpose, one must solve the secular equation pertaining to the operators A_1, A_2, and A_3 to determine the eigenvalues (relaxation rates) and to calculate the corresponding eigenoperators in the first approximation (*27*). After some tedious, but straightforward, algebra, the resulting rates and eigenoperators take on the form

$$R_S^{1\rho} = J_1 + J_2 \quad B_S = -\sqrt{\frac{5}{3}} A_1 + A_2$$

$$R_{F\mp}^{1\rho} = p \mp \sqrt{q^2+r^2}$$

$$B_\mp = -\frac{1}{\sqrt{2}}\left[\frac{\left(\omega_Q^4+\omega_Q^2\omega_1^2+4\omega_1^4\right) r \pm \lambda_1\lambda_2\left(\omega_Q^2-\omega_1^2\right)\sqrt{q^2+r^2}}{\lambda_1\lambda_2\left(\omega_Q^2-\omega_1^2\right) q + 6\omega_Q\omega_1^3 r}\right] A_1 + \sqrt{\frac{3}{10}}\left[\frac{2\lambda_1\lambda_2\omega_Q\omega_1 q - \left(\omega_Q^4+3\omega_1^2\omega_Q^2-4\omega_1^4\right) r \mp \lambda_1\lambda_2\left(\omega_Q^2+\omega_1^2\right)\sqrt{q^2+r^2}}{\lambda_1\lambda_2\left(\omega_Q^2-\omega_1^2\right) q + 6\omega_Q\omega_1^3 r}\right] A_2 + A_3 \quad [18]$$

with

$$p = \frac{3\omega_1^2}{2}\left(\frac{J_{\lambda_2}}{\lambda_2^2}+\frac{J_{\lambda_1}}{\lambda_1^2}\right) + \frac{3}{2}J_1 + \frac{3\left(\omega_Q^4+2\omega_1^2\omega_Q^2+8\omega_1^4\right)}{2\lambda_1^2\lambda_2^2} J_2 \qquad q = \frac{3\omega_1^2}{2}\left(\frac{J_{\lambda_2}}{\lambda_2^2}-\frac{J_{\lambda_1}}{\lambda_1^2}-\frac{4\omega_Q\omega_1}{\lambda_1^2\lambda_2^2} J_2\right)$$

$$r = \frac{(\omega_Q-2\omega_1)(\omega_Q+2\omega_1)}{2\lambda_1\lambda_2}(J_1+J_2). \quad [19]$$

In general, the central resonance shows a slow mode and two faster modes with rates $R_S^{1\rho}$ and $R_{F\mp}^{1\rho}$, respectively, because the spectral densities decrease in magnitude according to the order $J_{\lambda_2} \geq J_{\lambda_1} \geq J_1 \geq J_2$. The relative contributions (amplitudes) of the respective modes are determined by the eigenoperators B_S and $B_\mp$. The fast rates $R_{F\mp}^{1\rho}$ and the corresponding eigenoperators $B_\mp$ depend on the ratio of the spin-lock field strength and the static quadrupolar coupling ω_1/ω_Q. Slow dynamics is probed by the fast modes, because the rates $R_{F\mp}^{1\rho}$ are sensitive to the spectral densities $J_{\lambda 1} = J_0(\lambda_1)$ and $J_{\lambda 2} = J_0(\lambda_2)$ [note that they are insensitive to $J_0(0)$]. The slow relaxation rate $R_S^{1\rho}$ is sensitive to the high frequency contributions J_1 and J_2 only. Furthermore, $R_s^{1\rho}$ and the corresponding eigenoperator B_S (i.e., the relevant combination of A_1 and A_2) are insensitive to the relative strengths of the static interactions.

TABLE 3
Amplitudes in the Relaxation Functions of the Central Resonance Eq. [21]

	A_S	$A_{F\mp}$
$g_{11}(t)$	$\frac{1}{5}$	$\frac{1}{10}\left[\frac{\omega_Q^4+4\omega_Q^2\omega_1^2+64\omega_1^4}{\lambda_1^2\lambda_2^2}\pm\left(\frac{6\omega_Q^3\omega_1 q}{\lambda_1^2\lambda_2^2\sqrt{q^2+r^2}}+\frac{(\omega_Q+4\omega_1)(\omega_Q-4\omega_1)r}{\lambda_1\lambda_2\sqrt{q^2+r^2}}\right)\right]$
$g_{20}(t)$	0	$\frac{1}{2\sqrt{5}}\left[\frac{3\omega_Q\omega_1\left(\omega_Q^2+4\omega_1^2\right)}{\lambda_1^2\lambda_2^2}\pm\left(\frac{\left(\omega_Q^4-2\omega_Q^2\omega_1^2+16\omega_1^4\right)q}{\lambda_1^2\lambda_2^2\sqrt{q^2+r^2}}-\frac{3\omega_Q\omega_1 r}{\lambda_1\lambda_2\sqrt{q^2+r^2}}\right)\right]$
$g_{22}(t)$	0	$-\frac{\sqrt{3}}{2\sqrt{5}}\left[\frac{\omega_Q\omega_1\left(\omega_Q^2-4\omega_1^2\right)}{\lambda_1^2\lambda_2^2}\pm\left(\frac{2\omega_1^2\left(\omega_Q^2+8\omega_1^2\right)q}{\lambda_1^2\lambda_2^2\sqrt{q^2+r^2}}+\frac{\omega_Q\omega_1 r}{\lambda_1\lambda_2\sqrt{q^2+r^2}}\right)\right]$
$g_{31}(t)$	$-\frac{\sqrt{3}}{5\sqrt{2}}$	$-\frac{\sqrt{3}}{10\sqrt{2}}\left[\frac{\left(\omega_Q^4-6\omega_Q^2\omega_1^2-16\omega_1^4\right)}{\lambda_1^2\lambda_2^2}\pm\left(\frac{\omega_Q\omega_1\left(\omega_Q^2+20\omega_1^2\right)q}{\lambda_1^2\lambda_2^2\sqrt{q^2+r^2}}+\frac{\left(\omega_Q^2+4\omega_1^2\right)r}{\lambda_1\lambda_2\sqrt{q^2+r^2}}\right)\right]$
$g_{33}(t)$	$\frac{1}{\sqrt{10}}$	$-\frac{1}{2\sqrt{10}}\left[\frac{\omega_Q^4-2\omega_Q^2\omega_1^2+16\omega_1^4}{\lambda_1^2\lambda_2^2}\pm\left(\frac{3\omega_Q\omega_1\left(\omega_Q^2+4\omega_1^2\right)q}{\lambda_1^2\lambda_2^2\sqrt{q^2+r^2}}+\frac{(\omega_Q+2\omega_1)(\omega_Q-2\omega_1)r}{\lambda_1\lambda_2\sqrt{q^2+r^2}}\right)\right]$

The conversion of $\hat{T}_{11}(a)$ into the central resonance of the various coherences takes on the form [in the arrow notation (*10*)]

$$\hat{T}_{11}(a) \rightarrow g_{11}(t)\hat{T}_{11}(a) + g_{20}(t)\hat{T}_{20} + g_{22}(t)\hat{T}_{22}(s) + g_{31}(t)\hat{T}_{31}(a) + g_{33}(t)\hat{T}_{33}(a), \quad [20]$$

with the real (nonoscillating) relaxation functions

$$g_{ij}(t) = A_S \exp\left\{-R_S^{1\rho}t\right\} + A_{F-}\exp\left\{-R_{F-}^{1\rho}t\right\} + A_{F+}\exp\left\{-R_{F+}^{1\rho}t\right\}. \quad [21]$$

The factors (amplitudes) A_S and $A_{F\mp}$ are calculated with the eigenoperators in Eq. [18] and have been set out in Table 3. The time evolution of the other operators, pertaining to different initial states of the density operator, can analogously be derived. For each coherence, it was checked that the sum of the amplitudes of the slow and the fast modes (i.e., the integrated intensity of the central resonance) agrees with the relevant terms in Table 2. It is interesting that the conversions into the quadrupolar spin polarization $\hat{T}_{20}$ and the rank-two double-quantum coherence $\hat{T}_{22}(s)$ are bimodal, i.e. $g_{20}(t)$ and $g_{22}(t)$ do not exhibit a slow mode ($A_S = 0$). Furthermore, as will be discussed below, the latter two coherences are only excited if the ratio ω_1/ω_Q is of the order of unity. These features are particularly promising from an experimental point of view, because these coherences are only excited in the presence of a static quadrupolar coupling and bimodal lineshapes are easier to analyze than a trimodal resonance. As in the case of $R_S^{1\rho}$, the amplitude of the slow mode does not depend on the spin-lock field strength or the value of the static quadrupolar coupling. This is because the corresponding eigenoperator B_S is insensitive to these static interactions. For the fast modes, the amplitudes depend on the ratio ω_1/ω_Q as well as the spectral densities through the parameters q and r. In the limit $q \rightarrow 0$ and/or $r \rightarrow 0$ the dependencies of the amplitudes on the spectral densities are seen to vanish and the expressions are considerably simplified. These limiting situations correspond to some specific experimental conditions.

According to Eq. [19], the limit $r \rightarrow 0$ is realized when the high frequency spectral densities J_1 and J_2 dwindle and/or if $\omega_1 = \omega_Q/2$. Varying the RF field strength can always fulfill the latter condition, but the matching can become problematic in the face of B_1 inhomogeneity. The former situation is difficult to achieve because the high frequency spectral densities can usually not be neglected. For $\omega_1 = \omega_Q/2$, the fast rates read

$$\begin{aligned} R_{F-}^{1\rho} &= \frac{1}{4}J_{\lambda_1} + \frac{3}{2}J_1 + \frac{5}{4}J_2 \\ R_{F+}^{1\rho} &= \frac{3}{4}J_{\lambda_2} + \frac{3}{2}J_1 + \frac{3}{4}J_2 \end{aligned} \qquad (\omega_1 = \omega_Q/2,\ \lambda_1 = 2\sqrt{3}\omega_1,\ \lambda_2 = 2\omega_1) \quad [22]$$

and the amplitudes are set out in Table 4. Both fast relaxation rates are accessible, due to the nonzero and fixed values of the amplitudes. The resulting lineshapes have a relatively simple form and are suitable for fitting (although the condition $\omega_1 = \omega_Q/2$ limits the range of applicability).

TABLE 4
Amplitudes of the Fast Modes in the Relaxation Functions of the Central Resonance Eq. [21] in Some Specific Situations

	$\omega_1 \ll \omega_Q$ $(q=0)$		$\omega_1 = \omega_Q/2$ $(r=0)$		$\omega_1 \gg \omega_Q$ $(q=0)$	
	A_{F-}	A_{F+}	A_{F-}	A_{F+}	A_{F-}	A_{F+}
$g_{11}(t)$	$\frac{1}{5}$	0	$\frac{3}{10}$	$\frac{1}{10}$	$\frac{4}{5}$	0
$g_{20}(t)$	0	0	$\frac{3}{4\sqrt{5}}$	$\frac{1}{4\sqrt{5}}$	0	0
$g_{22}(t)$	0	0	$-\frac{\sqrt{3}}{4\sqrt{5}}$	$\frac{\sqrt{3}}{4\sqrt{5}}$	0	0
$g_{31}(t)$	$-\frac{\sqrt{3}}{5\sqrt{2}}$	0	$-\frac{\sqrt{3}}{20\sqrt{2}}$	$\frac{3\sqrt{3}}{20\sqrt{2}}$	$\frac{\sqrt{3}}{5\sqrt{2}}$	0
$g_{33}(t)$	$-\frac{1}{\sqrt{10}}$	0	$-\frac{3}{4\sqrt{10}}$	$\frac{1}{4\sqrt{10}}$	$-\frac{1}{\sqrt{10}}$	0

The other simplifying situation $q \to 0$ corresponds with the two limiting experimental conditions $\omega_1 \gg \omega_Q$ and $\omega_1 \ll \omega_Q$. In the former limit, the RF field strength far exceeds the static quadrupolar coupling and the frequencies collapse to the same value $\lambda_1 = \lambda_2 = 2\omega_1$ (the subset A_1, A_2, and A_3 is still decoupled from any other A_m). The corresponding rates of the fast modes now take on the values

$$\begin{aligned} R_{F-}^{1\rho} &= \frac{3}{4}J_{\lambda_1} + J_1 + \frac{1}{4}J_2 \\ R_{F+}^{1\rho} &= \frac{3}{4}J_{\lambda_2} + 2J_1 + \frac{5}{4}J_2 \end{aligned} \qquad (\omega_1 \gg \omega_Q, \lambda_1 = \lambda_2 = 2\omega_1) \qquad [23]$$

and the amplitudes are also collected in Table 4. The rate $R_{F+}^{1\rho}$ is however inaccessible, because $A_{F+} = 0$ for all coherences. For such strong RF field, the $\hat{T}_{20}$ and $\hat{T}_{22}(s)$ coherences are no longer excited and the central resonance of the other relevant coherences is now bimodal. In particular, outside the extreme narrowing limit, $\hat{T}_{31}(a)$ and triple-quantum $\hat{T}_{33}(a)$ coherences are created, despite the vanishing small static quadrupolar coupling with respect to the RF field strength. These results are in complete agreement with previous results derived under the neglect of a static quadrupolar coupling ($\omega_Q = 0$) in the doubly rotating tilted frame (*12–14*).

For very weak RF irradiation $\omega_1 \ll \omega_Q$, $\lambda_1 = \lambda_2 = \omega_Q$, one essentially spin-locks the central transition and the relaxation rates are no longer sensitive to the low frequency spectral densities:

$$\begin{aligned} R_{F-}^{1\rho} &= J_1 + J_2 \\ R_{F+}^{1\rho} &= 2J_1 + 2J_2 \end{aligned} \qquad (\omega_1 \ll \omega_Q, \lambda_1 = \lambda_2 = \omega_Q). \qquad [24]$$

According to the values of the amplitudes in Table 4, the only accessible rate is $R_{F-}^{1\rho}$ ($A_{F+} = 0$). Furthermore, the expression for $R_{F-}^{1\rho}$ equals the expression for $R_S^{1\rho}$ (see Eq. [18]) and, hence, the difference in slow and fast modes has disappeared (the relaxation functions are monoexponential). As far as the central resonance is concerned, only $\hat{T}_{11}(a)$ and $\hat{T}_{31}(a)$ single-quantum coherences are excited and the signal contributions pertaining to the zero- and multi-quantum coherences are seen to vanish ($\hat{T}_{33}(a)$ is no longer created because $A_S + A_{F-} = 0$). This behavior agrees with the previously derived results for spin $I = 3/2$ in a nonzero average electric field gradient without spin-lock field (*24*).

In the general case, the rates of the fast modes are given by the rather complicated results given in Eqs. [18]–[21] with the amplitudes collected in Table 3. In the next section we will compare the approximate analytic solutions with the solutions obtained from the numeric diagonalization and subsequent integration of the first set of coupled differential equations (i.e., the sum of Eqs. [8] and [13]). Furthermore, we will show the behavior of the fast modes for a specific form of the spectral density function with various correlation times and/or high frequency contributions.

THE FAST MODES

For a further analysis of the fast modes, it is necessary to introduce a specific form of the spectral density function. In biopolymer solutions there are often several independent processes at different time scales causing the loss of correlation (*2, 11*). Here, we will assume that there are two correlation times, a very short time τ_F and a longer time τ_S. The longer correlation time is associated with slow fluctuations in the (ordered) environment due to, e.g., rearrangements of relatively large macromolecular segments. The other very short correlation time is related to the dynamics of surrounding water molecules and/or other small ions, which typically occurs on a 10^{-12} s time scale. Accordingly, the fast process is taken to be in the extreme narrowing limit $\omega_0\tau_F \ll 1$. With a biexponential correlation function, the spectral density reads

$$\begin{aligned} J_m(\omega) &= \frac{(2\pi)^2}{20}\left(\frac{\chi_S^2\tau_S}{1+\omega^2\tau_S^2} + \chi_F^2\tau_F\right) \\ &= \frac{(2\pi)^2\chi_S^2\tau_S}{20}\left(\frac{1}{1+\omega^2\tau_S^2} + \alpha\right), \end{aligned} \qquad [25]$$

where χ_S and χ_F denote the root-mean-square coupling constants of the slow and fast process, respectively. We believe that this form of the spectral density function captures most of the specific effects, which may be encountered in experimental studies. The relative importance of the fast process (i.e., the high frequency contribution) is expressed by the parameter $\alpha = (\chi_F^2\tau_F)/(\chi_S^2\tau_S)$.

The fast rates are displayed vs ω_1/ω_Q in Fig. 2 for a number of scaled slow correlation times $\omega_Q\tau_S$. The rates are scaled by J_0 and are hence in dimensionless units. Here, there is no high frequency contribution to the spectral density ($\alpha = 0$). It

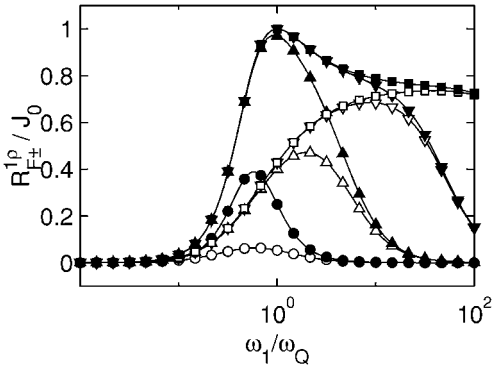

FIG. 2. Relaxation rates of the fast modes Eq. [18] scaled by J_0 vs the relative RF field strength ω_1/ω_Q. The symbols refer to the scaled correlation times: circles, $\omega_Q\tau_S = 1$; upper triangles, $\omega_Q\tau_S = 0.1$; lower triangles, $\omega_Q\tau_S = 0.01$; and squares, $\omega_Q\tau_S = 0.001$. Open and closed symbols denote $R^{1\rho}_{F-}$ and $R^{1\rho}_{F+}$, respectively. There is no high frequency contribution to the spectral density ($\alpha = 0$).

was checked that the approximate solutions resulting from the perturbation treatment Eqs. [18] and [19] are indiscernible from the rates obtained from the numerically solved time-evolution Eqs. [8] and [13] (the satellites do not overlap with the central resonance). If the high frequency contribution is negligible, the rates vary with increasing RF field strength according to $3\omega_1^2/\lambda_1^2 J_{\lambda 1}$ and $3\omega_1^2/\lambda_2^2 J_{\lambda 2}$ for $R^{1\rho}_{F-}$ and $R^{1\rho}_{F+}$, respectively. For stronger RF field strengths, the rates display a maximum and eventually level off at $3/4 J_0(2\omega_1)$. The position of the maximum depends on the value of the correlation time. However, the RF field strength dependence of the fast rates becomes far more complicated if the high frequency contribution to the spectral density cannot be neglected.

The importance of the spectral density at high frequencies, as expressed by the parameter α, is illustrated in Fig. 3. Note that the actual value of the Larmor frequency is irrelevant, because the fast relaxation process is assumed to be in the extreme narrowing limit ($\omega_0\tau_F \ll 1$). The rates (scaled by J_0) are displayed vs ω_1/ω_Q for a fixed slow correlation time $\omega_Q\tau_S = 0.1$. As for the amplitudes (see below), the perturbation results agree with the solutions resulting from numeric diagonalization and integration of the master equation. The high frequency contribution has a dramatic effect on the rates. In particular, when α exceeds, say, unity, a rather abrupt change is observed at $\omega_1 = \omega_Q/2$. This is related to the increasing importance of the parameter r (Eq. [19]) with increasing values of J_1 and J_2. As will be discussed below, similar critical behavior is observed in the amplitudes. The relaxation rates agree with Eqs. [22], [23], and [24] for the specific conditions $\omega_1 = \omega_Q/2$, $\omega_1 \gg \omega_Q$, and $\omega_1 \ll \omega_Q$, respectively.

The amplitudes of the fast modes are displayed vs ω_1/ω_Q in Figs. 4–8 for $\omega_Q\tau_S = 0.1$ and a number of values of α. With a shorter scaled slow correlation time $\omega_Q\tau_S$, the amplitudes take their limiting values for stronger RF fields (data not shown). The general behavior is however similar to the one displayed

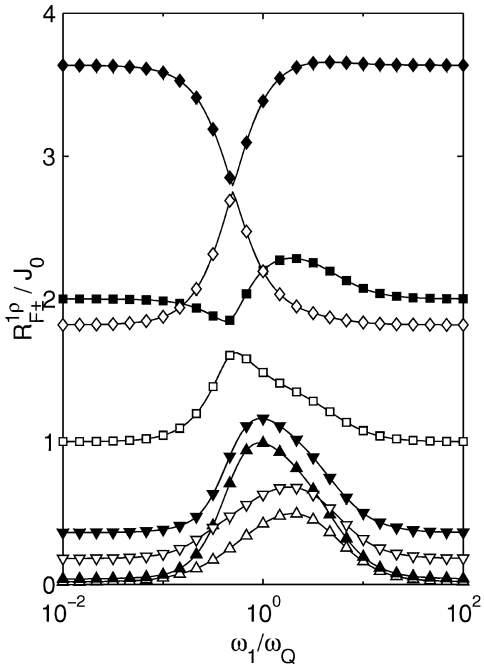

FIG. 3. As in Fig. 2, but for a fixed scaled correlation time $\omega_Q\tau_S = 0.1$ and high frequency contributions to the spectral density: upper triangles, $\alpha = 0.01$; lower triangles, $\alpha = 0.1$; squares, $\alpha = 1$; and diamonds, $\alpha = 10$.

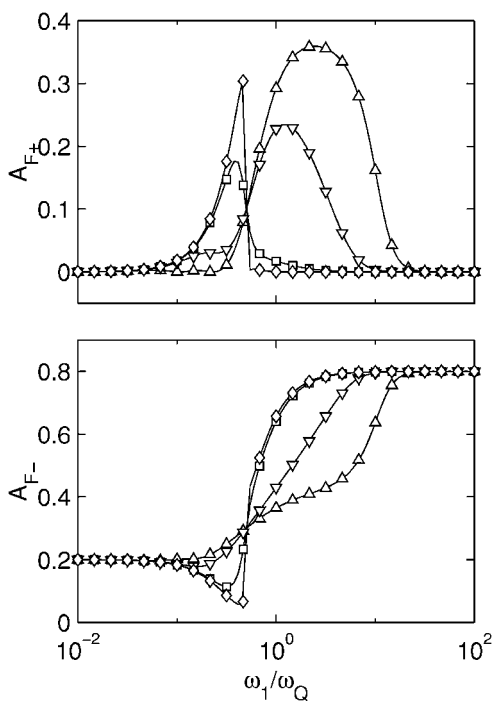

FIG. 4. Amplitudes of the fast modes (top) A_{F+} and (bottom) A_{F-} in the central resonance component of the $\hat{T}_{11}(a)$ coherence $[g_{11}(t)]$ vs the relative RF field strength ω_1/ω_Q with a fixed scaled correlation time $\omega_Q\tau_s = 0.1$. The symbols refer to the high frequency contributions to the spectral density: upper triangles, $\alpha = 0.01$; lower triangles, $\alpha = 0.1$; squares, $\alpha = 1$; and diamonds, $\alpha = 10$.

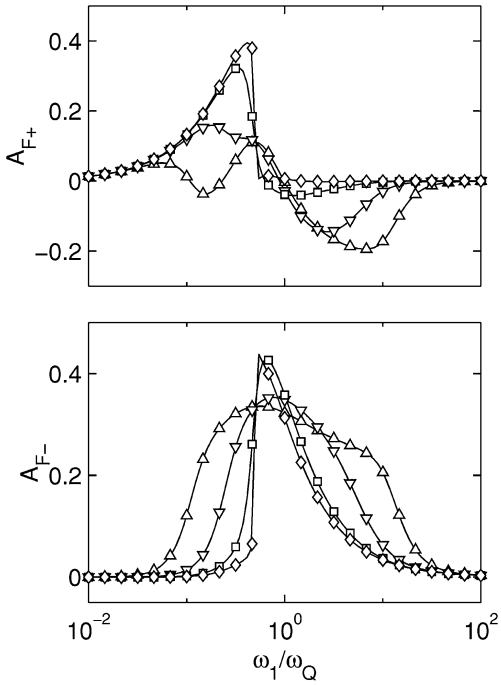

FIG. 5. As in Fig. 4, but for the $\hat{T}_{20}$ coherence [$g_{20}(t)$].

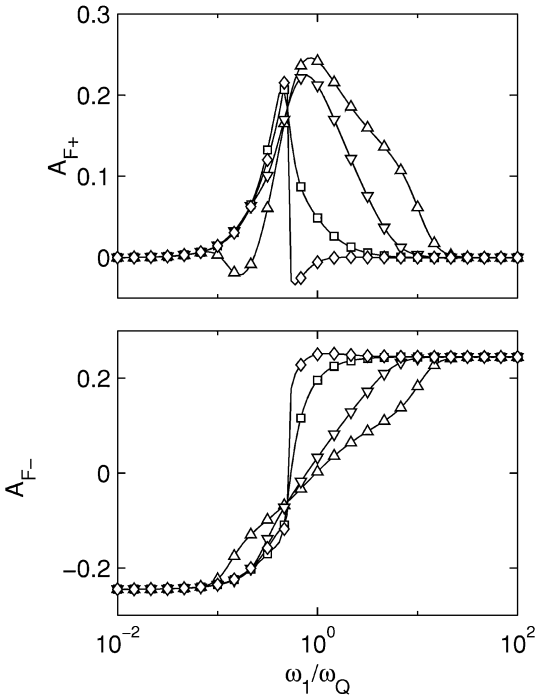

FIG. 7. As in Fig. 4, but for the $\hat{T}_{31}(a)$ coherence [$g_{31}(t)$].

in Figs. 4–8. Accordingly, the amplitudes are rather insensitive to the value of the slow correlation time. In contrast, the spectral density at high frequencies has a strong effect, except for $\omega_1 = \omega_Q/2$, $\omega_1 \gg \omega_Q$, or $\omega_1 \ll \omega_Q$. For the latter settings, the dependencies on the spectral densities vanish, in accordance with the results set out in Table 4. The two fast modes are only simultaneously observable if ω_1/ω_Q equals unity within an order of magnitude. For higher RF field strength, the amplitudes take their limiting values (Table 4) and the central resonance either vanishes [$\hat{T}_{20}$ and $\hat{T}_{22}(s)$] or becomes bimodal [$\hat{T}_{11}(a)$, $\hat{T}_{31}(a)$,

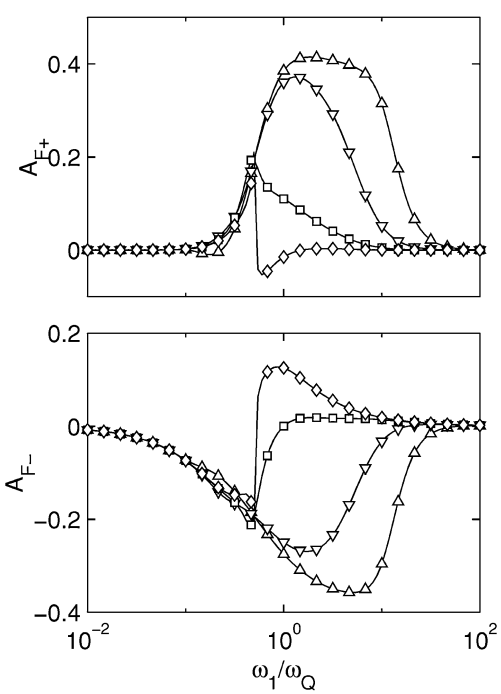

FIG. 6. As in Fig. 4, but for the $\hat{T}_{22}(s)$ coherence [$g_{22}(t)$].

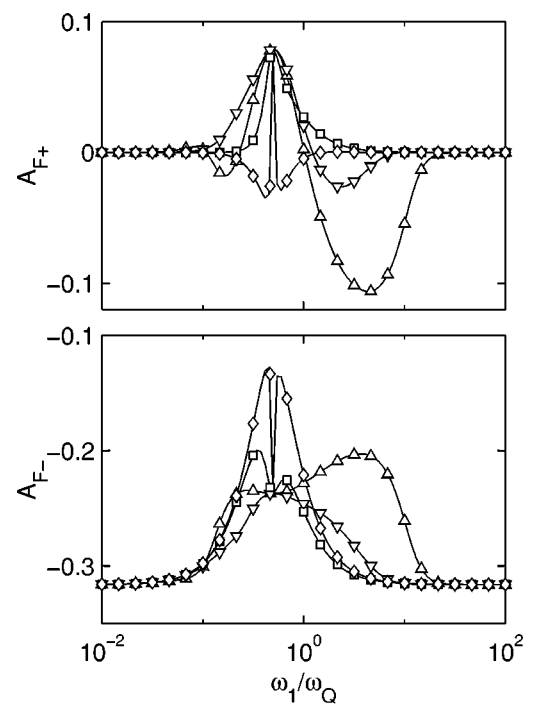

FIG. 8. As in Fig. 4, but for the $\hat{T}_{33}(a)$ coherence [$g_{33}(t)$].

and $\hat{T}_{33}(a)$]. As in the case of the rates, the amplitudes show an abrupt change at $\omega_1 = \omega_Q/2$ when α exceeds, say, unity.

PRACTICAL CONSIDERATIONS

The general pulse sequence of a spin-lock experiment is given by

$$(\pi/2)_{\phi+90} - (B_1, t_1)_{\phi} - (\beta)_{\phi'} - \text{ detection, } t_2, \qquad [26]$$

where the final pulse is possibly included for coherence transfer. Note that the filter contains a single transfer pulse only and not the conventional pulse-pair at the end of the evolution period. It is not necessary to include a mixing pulse, because the multiple-quantum coherences are already excited during the evolution under the lock. An initial (hard) pulse followed by a 90° phase shift is necessary to prepare the density operator in an initial state belonging to the relevant subset in Eqs. [8] and [13]. In the detection period, the relevant single-quantum coherences evolve into (detectable) $\hat{T}_{11}(a)$ coherence according to (*24*)

$$\begin{aligned}
\hat{T}_{11}(a) &\rightarrow \frac{1}{5}[3\cos(\omega_Q t_2)\exp(-R_s t_2) + 2\exp(-R_c t_2)]\hat{T}_{11}(a) \\
\hat{T}_{21}(s) &\rightarrow i\sqrt{\frac{3}{5}}\sin(\omega_Q t_2)\exp(-R_s t_2)\hat{T}_{11}(a) \qquad [27] \\
\hat{T}_{31}(a) &\rightarrow \frac{1}{5}\sqrt{6}[\cos(\omega_Q t_2)\exp(-R_s t_2) - \exp(-R_c t_2)]\hat{T}_{11}(a),
\end{aligned}$$

with $R_s = J_0 + J_1 + J_2$ and $R_c = J_1 + J_2$ being the transverse relaxation rates of the satellites and the central resonance (without spin-lock field), respectively. It is advisable to do two-dimensional (2D) experiments, either with or without coherence transfer. A set of spectra is obtained as a function of the spin-lock time t_1, after Fourier transformation with respect to the detection time t_2[$F(\omega_2)$ domain]. A phase sensitive 2D spectrum can now be obtained by taking the real part of this set and subsequent Fourier transformation with respect to the spin-lock time t_1. The signals in the $F(\omega_1)$ domain, pertaining to a certain static quadrupolar interaction, can be selected by taking a section along $F(\omega_1)$ at the position of the corresponding satellite signal in $F(\omega_2)$. This procedure is especially facilitated in the zero- and double-quantum filtered experiments, because these signals do not exhibit a central line in the $F(\omega_2)$ domain (see below).

Without final coherence transfer pulse (i.e., in a conventional spin-lock experiment), the detected signal includes $\hat{T}_{11}(a)$, $\hat{T}_{21}(s)$, and $\hat{T}_{31}(a)$ single-quantum coherences. After 2D Fourier transformation, the central resonance in the $F(\omega_1)$ domain contains the signal contributions originating from $\hat{T}_{11}(a)$ and $\hat{T}_{31}(a)$. The contribution related to $\hat{T}_{21}(s)$ is transformed into two satellite pairs in anti-phase in $F(\omega_1)$ and does not contribute to the central resonance [in $F(\omega_1)$]. Accordingly, the locked $\hat{T}_{11}(a)$ coherence converts into

$$\hat{T}_{11}(a) \rightarrow g_{11}(t_1)\hat{T}_{11}(a) + g_{31}(t_1)\hat{T}_{31}(a), \qquad [28]$$

which further evolves into detectable magnetization during the detection period. With Eq. [27], the directly detected signal takes the form

$$\begin{aligned}
s(t_1, t_2) = \frac{1}{5}[&(3g_{11}(t_1) + \sqrt{6}g_{31}(t_1))\cos(\omega_Q t_2)\exp(-R_s t_2) \\
&+ (2g_{11}(t_1) - \sqrt{6}g_{31}(t_1))\exp(-R_c t_2)]. \qquad [29]
\end{aligned}$$

The $T_{1\rho}$ relaxation of the satellites and central transition in $F(\omega_2)$ is readily identified in the first and the second term on the right-hand side of Eq. [29], respectively. For the satellites, the amplitude of the slow mode A_S is seen to vanish in the relevant combination of the relaxation functions $3g_{11} + \sqrt{6}g_{31}$ (see Table 3). Accordingly, the $T_{1\rho}$ relaxation of the satellites is bimodal and is sensitive to the fast modes only. Finally, the higher rank contributions are seen to vanish if one records the (extrapolated) amplitude of the detected signal directly after the spin-lock pulse ($t_2 \rightarrow 0$), or, alternatively, if one integrates the complete spectrum in the$F(\omega_2)$ domain.

The spin-lock experiment can be optimized to selectively detect the spin polarization quadrupolar order $\hat{T}_{20}$, the double-quantum coherences $\hat{T}_{22}(s)$ and $\hat{T}_{32}(a)$, or the triple-quantum coherence $\hat{T}_{33}(a)$. The other zero- and multi-quantum coherences belong to the other subset and are irrelevant in the context of the spin-lock experiment (they also do not exhibit a central line in the $F(\omega_1)$ domain). In particular, the selective detection of $\hat{T}_{22}(s)$ or $\hat{T}_{20}$ is interesting from an experimental point of view, because the corresponding central resonance signals [in $F(\omega_1)$] are bimodal and are sensitive to the fast relaxation modes only. As we will see below, in particular the signal pertaining $\hat{T}_{20}$ is most suitable to extract information about the low frequency behavior of the spectral density function and to selectively detect spin $I = 3/2$ nuclei in a nonzero average electric field gradient.

In the coherence transfer experiments, the final transfer pulse and the various phases should take on the following values:

(i) For optimized detection of the spin polarization quadrupolar order $\hat{T}_{20}$, the final coherence transfer pulse should read $\beta = 45°$. To suppress coherences up to and including order 3, the phase ϕ is stepped through 0°, 60°, 120°, 180°, 240°, and 300° while the receiver phase is kept at a constant value. Because of the invariance of $\hat{T}_{20}$ with respect to a rotation about the z axis, the value of the phase ϕ' of the coherence transfer pulse is irrelevant. Due to imperfections in the preparation pulse and subsequent 90° phase shift, Zeeman order $\hat{T}_{10}$ and octopolar spin polarization $\hat{T}_{30}$ may also be excited. Their signal contributions can however be suppressed by performing two experiments with coherence transfer pulse angles $\beta = 45°$ and 135°, respectively, and subsequent subtraction of the resulting spectra. For a single pulse angle, the same effect can be achieved if one takes the

difference of the sections at the resonance positions of the two satellites in the acquisition domain (see below).

(ii) In the triple-quantum filtration experiment, $\beta = 90^\circ$. The phase ϕ is also stepped through 0°, 60°, 120°, 180°, 240°, and 300°, but the receiver phase should now be alternated between 0° and 180°. Here, the phase ϕ' of the final pulse is set to 0° for selective detection of $\hat{T}_{33}(a)$ (the experiment is optimized for the unwanted $\hat{T}_{33}(s)$ coherence if $\phi' = 30^\circ$).

(iii) In the double-quantum filtration experiment, the phase ϕ is stepped through the values 0°, 90°, 180°, and 270° with the receiver phase being alternated between 0° and 180°. The phase ϕ' is set to 45° for selective, simultaneous, detection of $\hat{T}_{22}(s)$ and $\hat{T}_{32}(a)$ (the other combinations are selectively detected if $\phi' = 0^\circ$). A double-quantum filtered 2D spectrum with optimized pulse angle $\beta = 90^\circ$ displays two signal contributions: $\hat{T}_{22}(s)$ and $\hat{T}_{32}(a)$. The latter contribution does not exhibit a central resonance in $F(\omega_1)$ and is hence irrelevant from a relaxation analysis point of view. The $\hat{T}_{32}(a)$ coherence contribution can be suppressed however (at the cost of S/N ratio) by decreasing the length of final coherence transfer pulse such that $\beta = \arccos(1/\sqrt{3}) = 54.7^\circ$.

These phase cycles are possibly supplemented with a phase alternation of the preparation pulse between $+90^\circ$ and -90° together with an additional 180° alternation of the receiver phase. In the experimental section, we will demonstrate the feasibility of these coherence transfer experiments.

The preparation of the density operator depends on the RF field strength of the initial pulse in Eq. [26]. A pure $\hat{T}_{11}(a)$ initial state can only be prepared if the effects of relaxation and the static quadrupolar interaction can be neglected during a sufficiently hard preparation pulse. If this cannot be realized experimentally, the initial density operator after the phase shift will be in a mixed state including $\hat{T}_{10}$, $\hat{T}_{30}$, $\hat{T}_{11}(a)$, $\hat{T}_{21}(s)$, $\hat{T}_{22}(s)$, $\hat{T}_{31}(a)$, $\hat{T}_{32}(a)$, and $\hat{T}_{33}(a)$ coherences. The subsequent relaxation of the central resonance under the RF lock is still given by the rates in Eqs. [18] and [19], but the amplitudes of the various modes will be different from those collected in Table 3. Although the amplitudes can be derived analytically, it is more convenient to calculate them with a numeric integration of the master equation (including the effects of the preparation and coherence transfer pulses and the phase-shifts). It was checked however that under any circumstances the evolutions into $\hat{T}_{20}$ and $\hat{T}_{22}(s)$ coherences do not exhibit a slow mode and remain bimodal.

EXPERIMENT

Experiments have been done on spin $I = 3/2$ sodium in a dense (250 mg/ml), cholesteric, liquid crystal of 150 base-pair DNA fragments in water. This system has previously been investigated with extensive field-dependent longitudinal and transverse relaxation experiments (*2*). At 273 K, the sodium resonance shows a moderate static quadrupolar splitting $\omega_Q/2\pi =$ 550 Hz. The NMR experiments were done with a Bruker AM-200 spectrometer equipped with a 4.7 T wide-bore superconducting magnet and a fast recovery preamplifier. A homemade probe with a solenoid coil was used. To minimize dielectric heating due to parasitic capacitance during RF irradiation, a Faraday shield (consisting of a set of parallel, isolated, wires) was mounted inside the coil and at one side connected to ground. The sample was contained in a nonspinning 5-mm outer diameter and 1.5-cm length glass tube. The temperature was controlled at 273 K with a fluid thermostat using Fluorinert grade FC-40 (3M Co.). The hard $(\pi/2)$ pulse duration was 9 μs, whereas the spin-lock field intensity was tuned between 0.2 and 5 kHz using a Bruker BFX-5 low power transmitter. The RF carrier was adjusted exactly on resonance. For each experiment, 128 FIDs were collected with an incremental spin-lock time 165 μs. A 20 Hz Lorentzian line broadening was applied prior to Fourier transformation with respect to the spin-lock time.

Since the static quadrupolar coupling is rather moderate, the limiting situation $\omega_1/\omega_Q \gg 1$ can be achieved for the highest available spin-lock field strength $\omega_1/2\pi = 5$ kHz. In this situation, the conventional $T_{1\rho}$ relaxation of the spin-locked magnetization $[\hat{T}_{11}(a)]$ is almost biexponential with amplitudes $A_{F-} = 0.8$, $A_s = 0.2$ and rates $R^{1\rho}_{F-} = 3/4J_0(2\omega_1) + J_1 + 1/4J_2$, $R^{1\rho}_s = J_1 + J_2$, respectively (Table 4 and Eq. [23] with $\lambda_1 \approx \lambda_2 \approx 2\omega_1$). The high frequency contributions J_1 and J_2 were obtained from an inversion recovery experiment and take the values 130 and 110 s^{-1}, respectively (*28*). With the present spin-lock field strength and sweep width in the F_1 domain (6.06 kHz) the satellites are not observable. The rates were fitted to the data and the low frequency spectral density can now be derived from the fast relaxing component and reads $J_0(2\omega_1) = 310\ s^{-1}$ ($\omega_1/2\pi =$ 5 kHz).

In the presence of a large static quadrupolar coupling, the limiting situation $\omega_1/\omega_Q \gg 1$ can possibly not be achieved due to limited RF power. The conventional $T_{1\rho}$ relaxation experiment is now less eligible to extract dynamic information, because the relaxation functions become trimodal with rather complicated dependencies of the rates and amplitudes on the spin-lock field strength. It is now advisable to monitor the evolutions into the spin polarization quadrupolar order $\hat{T}_{20}$ or the double-quantum $\hat{T}_{22}(s)$ coherences, since these evolutions are sensitive to the fast relaxation rates only and are bimodal. Furthermore, the latter two coherences can only be excited in the presence of a static quadrupolar coupling and, hence, makes it possible to discern nuclei in anisotropic environment from those experiencing a zero average electric field gradient. We will now demonstrate the feasibility of the coherence transfer experiments and investigate to what extent the low frequency spectral densities can be obtained with limited RF power as well.

An experimental zero-quantum filtered 2D spectrum pertaining to the $\hat{T}_{20}$ coherence is shown in Fig. 9. The spectrum was recorded with a relatively moderate RF field strength $\omega_1/\omega_Q = 0.7$. A characteristic satellite pair in anti-phase in $F(\omega_2)$ with a splitting $\omega_Q/2\pi = 550$ Hz is observed, which is

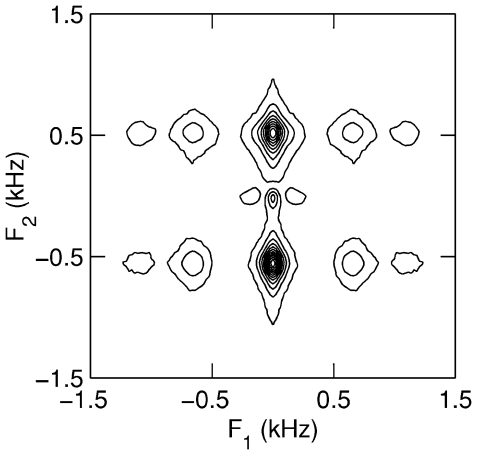

FIG. 9. Experimental 2D contour spectrum of the selectively detected quadrupolar order $\hat{T}_{20}$ in a dense DNA liquid crystal (at 273 K). Experimental parameters: $\omega_1/\omega_Q = 0.7$ and $\omega_Q/2\pi = 550$ Hz. The absolute value of the spectrum is displayed. The feature at the center is due to pulse-phase imperfections.

characteristic of the evolution of rank-two single-quantum coherence into observable magnetization during the detection period (see Eq. [27], in the figure the phase information is lost, because the absolute value of spectrum is displayed). Apart from the central resonance, the spectrum displays the two characteristic satellite pairs at frequencies $\lambda_1/2\pi$ and $\lambda_2/2\pi$ in $F(\omega_1)$ at the satellite positions in $F(\omega_2)$. The positions of the satellites in $F(\omega_1)$ agree with the spin-lock field strength and the value of the static quadrupolar coupling.

Figures 10 and 11 display the difference of the sections along $F(\omega_1)$ at the satellite positions in $F(\omega_2)$ for a variety of 2D experimental spectra. In Fig. 10, the experiments were optimized to selectively detect $\hat{T}_{20}$ (as in Fig. 9), the double-quantum coherence $\hat{T}_{22}(s)$, or the triple-quantum coherence $\hat{T}_{33}(a)$ with a fixed value of the spin-lock field strength $\omega_1/\omega_Q = 1.3$. Figure 11 shows the selectively detected $\hat{T}_{20}$ coherence for a range of relative RF field strengths ω_1/ω_Q. The relative intensity of the spectrum pertaining to the $\hat{T}_{22}(s)$ coherence with respect to the intensities of the other coherences is rather small, because in the double-quantum filtered experiment the coherence transfer pulse angle was decreased to the magic angle 54.7° for suppression of the unwanted $\hat{T}_{32}(a)$ coherence signal. The central resonance in the $\hat{T}_{33}(a)$ spectrum exhibits a strong, relatively narrow, Lorentzian component pertaining to the slow mode. In accordance with theory, the slow mode is absent in the central resonance of the selectively detected $\hat{T}_{20}$ and $\hat{T}_{22}(s)$ spectra and their shapes are sensitive to the fast modes only. The position of the satellites is very sensitive to the spin-lock field strength and the splitting increases with increasing RF power. Furthermore, they are particularly prone to inhomogeneous line broadening because of the inhomogeneity in the spin-lock field.

The $\hat{T}_{20}$ spectra in Figs. 10 and 11 are supplemented with simplex fits of the numerically solved time-evolution Eqs. [8] and [13], in which the spin-lock field strengths and inhomogeneity, as well the spectral density are optimized. As a first approximation, it is assumed that the inhomogeneous broadening of the satellites at the frequencies λ_i ($i = 1,2$) is related to the B_1 inhomogeneity $\Delta\omega_1$ according to $\Delta\omega_{\lambda_i} = |\partial\lambda_i/\partial\omega_1|\Delta\omega_1$. In the numerical procedure, the satellites were accordingly convoluted with the relevant broadening factors. Furthermore, it was assumed that the spectral density shows no dispersion in the 0–5 kHz range. Accordingly, the $\hat{T}_{20}$ spectra were fitted with four adjustable parameters: an overall factor, a spin-lock field strength, a relative inhomogeneity $\Delta\omega_1/\omega_1$, and the low frequency spectral density $J_0(0) \approx J_0(\lambda_1) \approx J_0(\lambda_2)$. The high frequency spectral densities J_1 and J_2 were fixed at their values

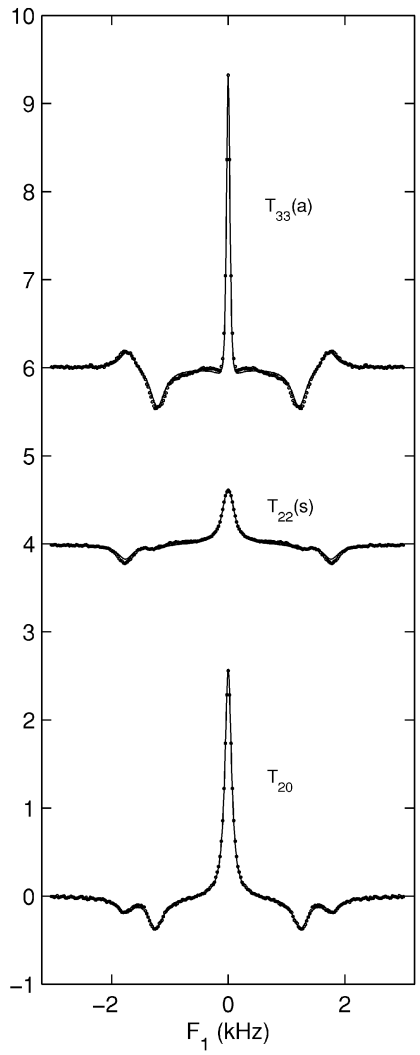

FIG. 10. Experimental sections (dots) along F_1 of the selectively detected (top) $\hat{T}_{33}(a)$, (middle) $\hat{T}_{22}(s)$, and (bottom) $\hat{T}_{20}$ coherences. For $\hat{T}_{22}(s)$ and $\hat{T}_{20}$ the difference of the sections at the resonance positions of the two satellites in F_2 are displayed. The spectra were recorded with a relative RF field strength $\omega_1/\omega_Q = 1.3$ ($\omega_Q/2\pi = 550$ Hz). The solid lines represent simplex fits. To avoid overlap, the spectra are shifted upward with 4 and 6 units for the double- and triple-quantum coherence, respectively.

obtained from an inversion recovery experiment. It should be noted that the spin-lock field strength and inhomogeneity determine the positions and widths of the satellites, respectively. The width of the central resonance is sensitive to one adjustable parameter only, i.e., the low frequency spectral density. For all spin-lock field strengths, the experimental $\hat{T}_{20}$ spectra are close to the fitted theoretical curves with a single relative inhomogeneous broadening $\Delta\omega_1/\omega_1 = 0.12$. The optimized spin-lock frequencies and spectral densities are collected in Table 5. The low frequency spectral density does not show a systematic variation, which confirms our conjecture concerning the absence of dispersion in the corresponding frequency range (0–5 kHz). Furthermore, the average value $J_0(0) \approx J_0(\lambda_1) \approx J_0(\lambda_2) = 285 \pm 20$ s^{-1} agrees within experimental error with the value obtained with a strong spin-lock field without coherence transfer [$J_0(2\omega_1) = 310$ s^{-1} for $\omega_1/2\pi = 5$ kHz]. Table 5 also includes the amplitudes and rates of both fast modes resulting from the fit. With limited RF power, the central resonance becomes truly bimodal and a fit to a single Lorentzian is clearly not sufficient.

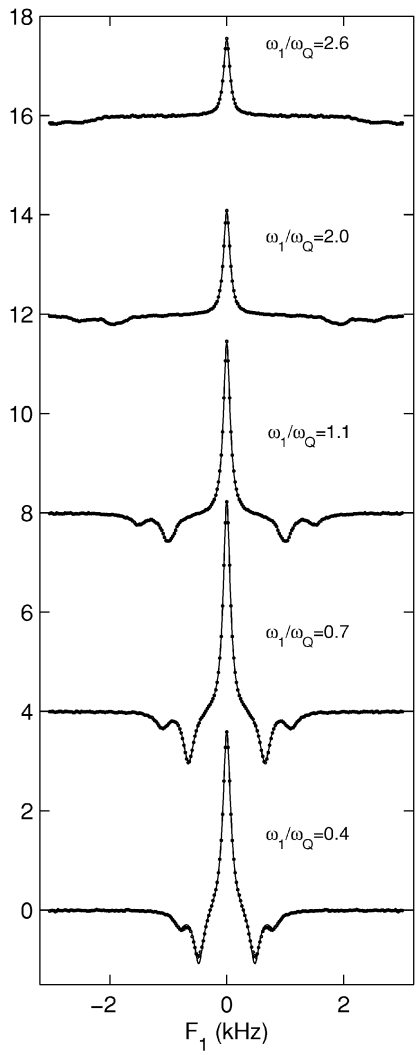

FIG. 11. Experimental sections (dots) along F_1 of the selectively detected quadrupolar spin polarization $\hat{T}_{20}$ for various relative RF field strengths ω_1/ω_Q as indicated in the figure. The solid lines represent simplex fits. To avoid overlap, the spectra are shifted upward with an increment of 4 units.

TABLE 5

Parameters Resulting from the Simplex Fit to the Selectively Detected Spin Polarization $\hat{T}_{20}$ Spectra ($\omega_Q/2\pi = 550$ Hz, $J_1 = 130$ s^{-1}, $J_2 = 110$ s^{-1})

ω_1/ω_Q	$J_0(0) = J_0(\lambda_1) = J_0(\lambda_2)$(s^{-1})	R_{F-}(s^{-1})	A_{F-}	R_{F+}(s^{-1})	A_{F+}
0.37	324	380	0.15	487	0.26
0.52	283	405	0.36	496	0.09
0.68	256	392	0.42	513	−0.01
0.84	272	391	0.40	552	−0.03
1.08	277	385	0.35	577	−0.05
1.33	302	396	0.31	609	−0.06
2.00	295	385	0.22	613	−0.05
2.56	279	372	0.17	603	−0.04

The spectra pertaining to the $\hat{T}_{22}(s)$ and $\hat{T}_{33}(a)$ coherences are less eligible to extract the dynamic information, because they are characterized by a rather small intensity [$\hat{T}_{22}(s)$] or a prominent narrow component [$\hat{T}_{33}(a)$]. In the fit of the latter two spectra, the low frequency spectral density was kept fixed at the average value 285 s^{-1}, whereas the spin-lock strength and inhomogeneity were optimized. As displayed in Fig. 10, excellent agreement between the fitted and experimental lineshapes is obtained with the same parameters as derived from the $\hat{T}_{20}$ spectra.

CONCLUSIONS

We derived analytic solutions to the previously deduced master equation describing the evolution of the spin quantum number $I = 3/2$ density operator in the presence of a RF field and both static and fluctuating quadrupolar interactions (*16*). In particular, the presence of a nonzero average electric field gradient has important consequences for the spin dynamics. The spectra resulting from Fourier transformation of the evolutions of the on-resonance spin-locked magnetization into the various coherences display two satellite pairs and, in some cases, a central line. From the approximate solutions, it results that the central line is generally trimodal, consisting of a narrow component related to a slowly relaxing mode and two broad components pertaining to two faster relaxing modes. Neither the amplitude nor the width of the narrow component is affected by the magnitude of the static coupling, whereas the characteristics of the broad components depend in a rather complicated manner on the relative spin-lock field strength with respect to the static quadrupolar interaction. One of the promising emerging features is the fact that the evolutions into the central lines of the selectively detected quadrupolar order and the rank-two double-quantum coherence do not exhibit a slow mode and are particularly sensitive to slow molecular motion. Furthermore, these coherences can only be

excited in the presence of a static coupling and this makes it possible to discern nuclei in anisotropic from those in isotropic environment. The feasibility of the (coherence transfer) spin-lock experiments to extract dynamic information with limited RF power and a static quadrupolar interaction has been demonstrated through experiments on sodium in a dense, cholesteric, DNA liquid crystal.

The present work may be consequential for at least three different experimental NMR methodologies. The first is the classical problem on how to extract the spectral densities from a variety of relaxation experiments and how to detect slow molecular motions in soft condensed matter. In our experimental example, we confirmed the absence of fluctuations in the kHz range, since the derived spectral densities comply with a slow correlation time 7 ns (*2*). A second issue is the monitoring of spin $I = 3/2$ nuclei in an anisotropic environment via the spin-lock experiment, through the selective detection of either the quadrupolar order or rank-two double-quantum coherence. These coherences are only created during the spin-lock time if there is a residual quadrupolar coupling in the sample, and if the applied spin-lock field has a comparable strength to this coupling. Since this method does not rely upon a flip angle effect for suppression of unwanted signal components, it may be desirable over the conventional DQ-MA filter (*5*, *19*, *20*). Finally, the magnitude of the sodium signal filtered through the quadrupolar order is comparable to the magnitude obtained with a triple-quantum filter. The triple-quantum filter is however particularly sensitive to ions involved in slow motion, irrespective the presence of a static, possibly hidden, quadrupolar coupling. If implemented in an imaging application, the further selectivity and sensitivity of the spin-lock filtering technique to sodium ions in an *ordered* environment might prove to be a valuable tool for the diagnosis of different diseases associated with loss of ordering of the sodium ions (*18*). Since in biological media the static quadrupolar splittings are rather small (<1 kHz), the RF power deposition in such an experiment would be minimal.

ACKNOWLEDGMENT

J. vdM acknowledges A. Delville for stimulating discussions.

REFERENCES

1. A. Delville, P. Porion, and A. M. Faugere, *J. Phys. Chem.* B **104,** 1546 (2000).
2. L. C. A. Groot, J. R. C. van der Maarel, and J. C. Leyte, *J. Phys. Chem.* **98,** 2699 (1994).
3. D. E. Woessner, *Concepts in Magn. Reson*., in press.
4. V. M. Stein, J. P. Bond, M. W. Capp, C. F. Anderson, and M. T. Record, *Biophys. J.* **68,** 1063 (1995).
5. U. Eliav and G. Navon, *J. Magn. Reson. B.* **103,** 19 (1994).
6. S. Hilal, C. Oh, I. Mun, and A. Silver, Sodium Imaging, *in* "Magnetic Resonance Imaging" (D. Stark and W. Bradley, Eds.), Mosby, St. Louis (1992).
7. T. Meersmann, S. A. Smith, and G. Bodenhausen, *Phys. Rev. Lett.* **80,** 1398 (1998).
8. F. Lurçat, *Comptes Rendus* **240,** 2517 (1955).
9. P. S. Hubbard, *J. Chem. Phys.* **53,** 985 (1970).
10. G. Jaccard, S. Wimperis, and G. Bodenhausen, *J. Chem. Phys.* **85,** 6282 (1986).
11. S. W. W. Chen and P. J. Rossky, *J. Phys. Chem.* **97,** 10803 (1993).
12. J. R. C. van der Maarel, *J. Chem. Phys*. **91,** 1446 (1989).
13. J. R. C. van der Maarel, R. H. Tromp, J. C. Leyte, J. H. Hollander, and C. E. Erkelens, *Chem. Phys. Lett.* **169,** 585 (1990).
14. J. R. C. van der Maarel, *J. Chem. Phys*. **94,** 4765 (1991).
15. I. Hancu, F. E. Boada, and G. Shen, *Magn. Reson. Med.* **42,** 1146 (1999).
16. I. Hancu, J. R. C. van der Maarel, and F. E. Boada, *J. Magn. Reson.* **147,** 179 (2000).
17. J. R. C. van der Maarel, *J. Chem. Phys*. **99,** 5646 (1993).
18. L. A. Jelicks, P. K. Paul, E. Obyrne, and R. K. Gupta, *J. Magn. Reson. Imag.* **3,** 565 (1993).
19. D. E. Woessner and N. Bansal, *J. Magn. Reson.* **133,** 21 (1998).
20. R. Kemp-Harper, S. Brown, C. Hughes, P. Styles, and S. Wimperis, *Prog. NMR Spectrosc.* **30,** 157 (1997).
21. R. Reddy, L. Bolinger, M. Shinnar, E. Noyszewski, and J. S. Leigh, *Magn. Reson. Med.* **33,** 134 (1995).
22. A. Abragam, "Principles of Nuclear Magnetism," Oxford University Press, New York (1978).
23. G. J. Bowden, W. D. Hutchinson, and J. Khachan, *J. Magn. Reson.* **67,** 415 (1986).
24. J. R. C. van der Maarel, *Chem. Phys. Lett.* **155,** 288 (1989).
25. G. Campolieti, B. C. Sanctuary, and H. B. R. Cole, *J. Magn. Reson.* **88,** 457 (1990).
26. T. R. J. Dinesen and B. C. Sanctuary, *J. Chem. Phys.* **101,** 7372 (1994).
27. L. D. Landau and E. M. Lifshitz, "Quantum Mechanics (Non-relativistic Theory), Course of Theoretical Physics," Vol. 3, 3rd ed., Pergamon Press, Oxford (1977).
28. The longitudinal relaxation rate of the satellites is monoexponential with rate $R_{1,s} = 2J_2$. The longitudinal rate of the central resonance is biexponential with equal fractions and rates $R_{1,c1} = J_1$ and $R_{1,c2} = J_2$. For a small difference in J_1 and J_2, the central line can be fitted to a single exponential with an average rate $R_{1,c} = J_1 + J_2$ (*24*).